Thermodynamic Basis of Electron Transfer in Dihydroorotate Dehydrogenase B from *Lactococcus lactis*: Analysis by Potentiometry, EPR Spectroscopy, and ENDOR Spectroscopy†

Al-Walid A. Mohsen,‡ Stephen E. J. Rigby,§ Kaj Frank Jensen,|| Andrew W. Munro,‡ and Nigel S. Scrutton*,‡

Department of Biochemistry, University of Leicester, Leicester LE1 7RH, U.K., Department of Biological Sciences, Queen Mary College, University of London, London E1 4NS, U.K., and Institute of Molecular Biology, University of Copenhagen, Solvgade 83H, Copenhagen DK-1307, Denmark

Received December 4, 2003; Revised Manuscript Received March 9, 2004

ABSTRACT: Dihydroorotate dehydrogenase B (DHODB) is a complex iron−sulfur flavoprotein that catalyzes the conversion of dihydroorotate to orotate and the reduction of NAD^+. The enzyme is a dimer of heterodimers containing an FMN, an FAD, and a 2Fe−2S center. UV−visible, EPR, and ENDOR spectroscopies have been used to determine the reduction potentials of the flavins and the 2Fe−2S center and to characterize radicals and their interactions. Reductive titration using dithionite indicates a five-electron capacity for DHODB. The midpoint reduction potential of the 2Fe−2S center (−212 ± 3 mV) was determined from analysis of absorption data at 540 nm, where absorption contributions from the two flavins are small. The midpoint reduction potentials of the oxidized/semiquinone (E_1) and semiquinone/hydroquinone (E_2) couples for the FMN ($E_1 = -301 \pm 6$ mV; $E_2 = -252 \pm 8$ mV) and FAD ($E_1 = -312 \pm 6$ mV; $E_2 = -297 \pm 5$ mV) were determined from analysis of spectral changes at 630 nm. Corresponding values for the midpoint reduction potentials for FMN ($E_1 = -298 \pm 4$ mV; $E_2 = -259 \pm 5$ mV) in the isolated catalytic subunit (subunit D, which lacks the 2Fe−2S center and FAD) are consistent with the values determined for the FMN couples in DHODB. During reductive titration of DHODB, small amounts of the neutral blue semiquinone are observed at ∼630 nm, consistent with the measured midpoint reduction potentials of the flavins. An ENDOR spectrum of substrate-reduced DHODB identifies hyperfine couplings to proton nuclei similar to those recorded for the blue semiquinone of free flavins in aqueous solution, thus confirming the presence of this species in DHODB. Spectral features observed during EPR spectroscopy of dithionite-reduced DHODB are consistent with the midpoint reduction potentials determined using UV−visible spectroscopy and further identify an unusual EPR signal with very small rhombic anisotropy and *g* values of 2.02, 1.99, and 1.96. This unusual signal is assigned to the formation of a spin interacting state between the FMN semiquinone species and the reduced 2Fe−2S center. Reduction of DHODB using an excess of NADH or dihydroorotate produces EPR spectra that are distinct from those produced by dithionite. From potentiometric studies, the reduction of the 2Fe−2S center and the reduction of the FMN occur concomitantly. The study provides a detailed thermodynamic framework for electron transfer in this complex iron−sulfur flavoprotein.

The dihydroorotate dehydrogenases (DHODs)[1] are a heterogeneous group of enzymes that catalyze the conversion of dihydroorotate to orotate and the transfer of electrons to various redox acceptors. These enzymes catalyze the only redox reaction in the pathway for the *de novo* biosynthesis of pyrimidines. Three enzyme groups have been identified: the class 1A enzymes which contain a FMN prosthetic group and are soluble, the class 1B enzymes which are also soluble and contain FMN, FAD, and a 2Fe−2S center, and the class 2 enzymes which are restricted to eukaryotes and Gram-negative bacteria, are membrane-bound, contain FMN, and are oxidized by ubiquinone. *Lactococcus lactis* and related milk-fermenting bacteria like *Enterococcus faecalis* are unusual in possessing two DHOD enzymes [DHODA (class 1A) and DHODB (class 1B)]. DHODB (EC 1.3.3.1) has been identified and purified from a number of organisms, including *L. lactis*, *Bacillus subtilis*, *En. faecalis*, and *Clostridium oroticum* (*1*−*4*), and the enzyme operates with NAD^+ as the electron acceptor (Scheme 1). The crystal structure of DHODB from *L. lactis* has been determined at 2.1 Å resolution, revealing a dimer of heterodimers comprising a catalytic subunit (termed subunit D) that is responsible for the oxidation of dihydroorotate to orotate and reduction of the subunit D-bound FMN cofactor (*5*), and two-electron

† This work was funded by grants from the BBSRC, the Wellcome Trust, and the Lister Institute of Preventive Medicine. N.S.S. is a Lister Institute Research Professor.

* To whom correspondence should be addressed. Telephone: +44 116 223 1337. Fax: +44 116 252 3369. E-mail: nss4@le.ac.uk.

‡ University of Leicester.

§ University of London.

|| University of Copenhagen.

[1] Abbreviations: DHOD, dihydroorotate dehydrogenase; FAD, flavin adenine dinucleotide; FMN, flavin mononucleotide; IPTG, isopropyl β-D-thiogalactoside.

10.1021/bi036179i CCC: $27.50
Published on Web 05/05/2004

Scheme 1

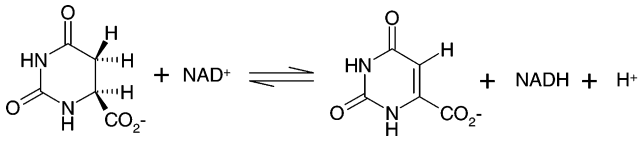

transfer subunits (termed subunit K) involved in electron transfer to NAD^+. Subunit K contains a 2Fe−2S center bound in a loop close to the subunit interface of the heterodimer. Subunit K also binds FAD, which transfers a hydride ion to the coenzyme NAD^+ after receiving electrons from the 2Fe−2S center. The crystal structure of DHODB determined in the presence of orotate indicates that conformational changes occur at specific regions of the catalytic subunit upon substrate binding (*5*). These include relatively large movements for the side chains of Lys-D48 and Tyr-K232, which might affect the electronic properties of the FMN and 2Fe−2S center, respectively. Other conformational changes that occur in a loop at the entrance to the active site of the catalytic subunit are large and might effect secondary changes that are difficult to characterize by X-ray crystallography. This contrasts with DHODA from *L. lactis* in which the binding of orotate does not induce significant conformational change (*6*).

Kinetic and mechanistic studies of the class 2 and 1A DHOD enzymes have been reported (*7*−*11*). Mechanistic information is also available for the more complex 1B DHOD enzymes. Kinetic isotope effects and pH kinetic data for *En. faecalis* DHODB have demonstrated that the reaction is reversible and that rate-limiting macroscopic ionizations attributed to one or more residue side chains are associated with the reductive and oxidative half-reactions (*4*). Similar studies with *C. oroticum* DHODB suggest that an active site cysteine and lysine residue act as a general base and electrostatic catalyst, respectively (*2*). Double isotope effects on ^{D}V and $^{D}(V/K_{DHO})$ obtained for deuteration at C_5-*proS* and C_6 of dihydroorotate are consistent with a mechanism in which C_5-*proS* proton transfer and C_6-hydride transfer are concerted. This concerted mechanism of substrate oxidation proceeds without formation of an unstable carbanion intermediate [$pK_a \sim 20-21$ (*12*)]. Herein, we report a thermodynamic study of *L. lactis* DHODB and characterization of the redox centers using EPR and ENDOR spectroscopy. A combination of UV−visible spectroscopy, potentiometry, and EPR and ENDOR spectroscopy has enabled us to determine the midpoint reduction potentials of the three redox centers in DHODB and to demonstrate spin coupling between the FMN and 2Fe−2S center. Our work establishes a firm thermodynamic basis for the reversible nature of electron transfer in DHODB and forms a platform for future detailed kinetic studies.

EXPERIMENTAL PROCEDURES

Materials. Most fine chemicals were obtained from Life Technologies Inc. (Paisley, U.K.). Ampicillin, *S*-dihydroorotic acid sodium salt, benzyl viologen, FAD, FMN, methyl viologen, NADH, orotic acid sodium salt, and phenazine methosulfate were obtained from Sigma (Poole, Dorset, U.K.). 2-Hydroxy-1,4-naphthoquinone was obtained from Aldrich.

Cell Culture and Enzyme Expression. Escherichia coli strain SØ6645 containing the pFN3 plasmid, which harbors the *pyrDb* and *pyrK* genes of *L. lactis* encoding DHODB catalytic (subunit D) and electron transfer (subunit K) subunits (*3*), respectively, was grown from an inoculum in 2 L flasks containing 1 L of 2-YT medium supplemented with 5 g/L K_2HPO_4, 4 mM $MgSO_4$, 100 μg/mL ampicillin, and 10 mL/L glycerol. After incubation overnight with continuous shaking at 28 °C, the temperature was reduced to 25 °C, FMN was added to a final concentration of 100 μM and ferrous sulfate to 0.2 g/L, and the cells were induced using 0.5 mM IPTG for 2 h. Cells were harvested by centrifugation, and the cell pellets obtained (typically 15−20 g/L of medium) from 6 L were combined and stored at −70 °C. *E. coli* strain SØ6645 containing the pFN2 plasmid, which harbors the *pyrDb* gene expressing the catalytic subunit D, was grown in 2-YT culture supplemented as described above. After incubation overnight with continuous shaking at 28 °C, the temperature was reduced to 25 °C and the cells were induced using 0.5 mM IPTG for 2 h. Cells were harvested by centrifugation, and the cell pellets obtained from 6 L were combined and stored at −70 °C.

Purification of DHODB. Cell paste was thawed and resuspended in 50 mM Tris-HCl buffer (pH 8) containing 0.1 mM FMN and 0.1 mM FAD, and the cell suspension was sonicated (8 × 40 s pulses using a 2.5 cm probe at 45% power). During sonication, the temperature was maintained at <15 °C by incubation of the suspension on ice, and the pH was maintained at 7 by addition of small amounts of Tris base (from a 2 M solution). Cell debris was removed by centrifugation (25000*g* for 35 min), and the supernatant was then dialyzed for 3 h against 7 L of 50 mM Tris-HCl buffer (pH 8) at 4 °C. The sample was applied to a Q-Sepharose HP column (26 cm × 2.6 cm) pre-equilibrated with 25 mM Tris-HCl buffer (pH 8) (buffer A). The column was washed using a 220 mL gradient of 8 to 22% buffer B [25 mM Tris-HCl buffer (pH 8) and 1 M NaCl], followed by 100 mL of 22% buffer B. A further gradient (600 mL from 22 to 32% buffer B in buffer A) was then used to develop the column. DHODB fractions with an absorbance ratio at 272 nm to 453 nm of <5.6 were pooled, and the amount of enzyme was estimated from its absorbance at 540 nm ($\epsilon = 5990\ M^{-1}\ cm^{-1}$). The pooled sample was desalted using a ceramic hydroxyapatite column (Bio-Rad). The enzyme bound to the resin in the presence of the NaCl and continued to bind after being washed with 90 mL of 25 mM Tris-HCl buffer (pH 8) and 250 mM NaCl. The enzyme was then eluted with 5 mM potassium phosphate (pH 7.6). The 272 nm/453 nm absorbance ratio of the pooled DHODB fractions was 3.9. Ammonium sulfate was added slowly to the pooled fractions from a 4 M solution to a final concentration of 1.6 M. The sample was centrifuged (26000*g* for 30 min) to remove precipitated material, and the supernatant was then applied to a Phenyl-Sepharose HP column (26 cm × 2.6 cm) equilibrated with 25 mM Tris-HCl buffer (pH 7.6) containing 1.6 M ammonium sulfate. The bound sample was washed with the same buffer, but containing 1.3 M ammonium sulfate, and then eluted using a gradient (500 mL) of ammonium sulfate from 1.2 to 0.7 M in the same buffer. The eluted DHODB (approximately 70 mg of protein) consistently had a 272 nm/453 nm absorbance ratio of approximately 3.15, and was obtained

in an essentially homogeneous form following these chromatographic steps. The protein was concentrated to >500 μM by ultrafiltration and stored at −80 °C.

Purification of the DHODB Catalytic Dimer (Subunit D). Cell paste (~80 g) was thawed and resuspended in 100 mM Tris-HCl buffer (pH 8) containing 0.5 mM FMN. The cell suspension was sonicated (8 × 40 s pulses using a 2.5 cm probe at 45% power). As with the preparation of DHODB, the temperature and pH were maintained at <15 °C and pH 7, respectively. Cell debris was removed by centrifugation (25000*g* for 35 min), and the sample was dialyzed for 3 h against 50 mM Tris-HCl buffer (pH 8) at 4 °C and then fractionated with ammonium sulfate (45%). The precipitate was redissolved in buffer A, dialyzed twice, for 3 h each, against the same buffer, and centrifuged to clarify the sample prior to being loaded on a Q-Sepharose HP column pre-equilibrated with buffer A. The column was further washed with 200 mL of the same buffer. The enzyme was eluted using a gradient (15% buffer B to 25% buffer B over 300 mL) followed by a final wash step (100 mL of 25% buffer B). Fractions with 272 nm/452 nm absorbance ratios of <4.7 were pooled and applied to Phenyl-Sepharose HP column pre-equilibrated with 50 mM Tris-HCl buffer (pH 8.0) containing 0.2 M ammonium sulfate. After being washed, the protein was eluted with a gradient (300 mL) of ammonium sulfate (from 0.1 to 0 M) contained in 50 mM Tris-HCl buffer (pH 8.0). Fractions with 272 nm/452 nm ratios of <3.9 were pooled, concentrated by ultrafiltration, and stored at −80 °C.

Anaerobic Reduction of DHODB with Substrates and Sodium Dithionite. All anaerobic experiments were carried out in Belle Technology gloveboxes equipped with either a Jasco V-550 UV−visible spectrophotometer or a fiber optic probe connected to an external Cary UV-50 Bio UV−visible spectrophotometer (Varian), and a Hanna pH211 microprocessor coupled to a Pt/Calomel electrode (Thermo-Russell Ltd.), for redox potential measurements. The atmosphere of the gloveboxes was maintained at <2 ppm oxygen. Most of the oxygen was removed from buffers by bubbling solutions with oxygen-free argon for 2 h prior to their introduction into the anaerobic glovebox. Residual oxygen was removed, and buffers were exchanged from the enzyme samples by gel filtration inside the gloveboxes using an Econo-Pac 10DG column from Bio-Rad (Hercules, CA). DHODB and the catalytic subunit (subunit D) were titrated with sodium dithionite under anaerobic conditions. The sodium dithionite solution was standardized by titration against a FAD solution with a known concentration (typically 50−100 μM). DHODB and the catalytic subunit were also reduced under anaerobic conditions with a 50 mM stock solution of either dihydroorotate or NADH prepared fresh in the glovebox. Upon each addition of either dihydroorotate or NADH, the enzyme/substrate mixture was allowed to equilibrate for 4 min prior to the acquisition of the absorption spectrum. All reductions were carried out in 50 mM potassium phosphate buffer (pH 7.0).

Redox Potentiometry. Anaerobic redox titrations were conducted with the enzyme (intact DHODB and the FMN-containing subunit D; typically at 30−100 μM) present in 100 mM potassium phosphate (pH 7.0). The protein sample was scrubbed free of oxygen as indicated above. Mediators for improved conductivity between the enzyme and electrode were added. Typically, these were (final concentrations) 2 μM phenazine methosulfate ($E_{1/2}$ = 80 mV vs SHE), 5 μM 2-hydroxy-1,4-naphthoquinone (−152 mV), 0.5 μM methyl viologen (450 mV), and 1 μM benzyl viologen (−358 mV), as described previously (*13*, *14*). Sodium dithionite or potassium ferricyanide was added in small volumes, typically 0.2−0.5 μL from stock solutions (1 and 10 mM), to reduce or oxidize, respectively, the enzymes. Adequate time was allowed for electronic equilibration following each addition of reductant or oxidant, prior to the spectrum being recorded at a stabilized reduction potential. Spectra were recorded between 300 and 800 nm using a fiber optic probe (Varian) immersed in the enzyme solution (typically approximately 7 mL of enzyme) and connected to a Cary UV-50 Bio spectrophotometer. The electrochemical potential was monitored using a Hanna pH211 microprocessor Pt/Calomel electrode at 25 ± 2 °C. The electrode was calibrated using the Fe^{3+}/Fe^{2+} EDTA couple as a standard (108 mV). Sodium dithionite and ferricyanide solutions were made up fresh inside the glovebox in the redox titration buffer immediately prior to the experiment. The enzyme was mixed slowly using a 8.5 mm magnetic flea on a magnetic stirrer throughout the experiments to expedite equilibration with the electrode. At least 60 spectra were collected in each experiment, covering the range between approximately −500 and 200 mV (vs the standard hydrogen electrode); +244 mV was factored into the potential reading obtained to correct for standard hydrogen electrode values.

Data manipulation and analysis were performed using Origin (Microcal). Absorbance data at wavelengths appropriate for monitoring the reduction and oxidation of the flavin cofactors (453 nm, near the oxidized maximum, and 630 nm, for the neutral blue semiquinone on the FMN cofactor) and the 2Fe−2S center (540 nm) were plotted against the relevant reduction potential (*15*). Absorption versus potential data for the FMN-containing subunit D were analyzed at both 453 and 630 nm. Data for DHODB were analyzed in addition at 540 nm, where an absorption change due to the reduction of the 2Fe−2S center occurred between approximately −100 and −350 mV (vs SHE). Data for the FMN cofactor in subunit D were fitted to eq 1, representing a two-electron redox process and derived by extension to the Nernst equation and the Beer−Lambert law, as described previously (*13*):

$$A = \frac{a \times 10^{(E-E_1')/59} + b + c \times 10^{(E_2'-E)/59}}{1 + 10^{(E-E_1')/59} + 10^{(E_2'-E)/59}} \quad (1)$$

A_{540} data between −100 and −300 mV for the titration of the DHODB heterodimer were fitted to eq 2, representing a one-electron process, to obtain an estimate for the reduction potential of the 2Fe−2S center.

$$A = \frac{a + b \times 10^{(E_1'-E)/59}}{1 + 10^{(E_1'-E)/59}} \quad (2)$$

DHODB heterodimer data at 453 nm were fitted to eq 3, representing a four-electron redox process, as described previously (*14*). DHODB heterodimer data at 630 nm were

also fitted to eq 3 to describe the formation and decay of semiquinone species on the flavin(s).

$$A = \frac{a \times 10^{(E-E_1')/59} + b + c \times 10^{(E_2'-E)/59}}{1 + 10^{(E-E_1')/59} + 10^{(E_2'-E)/59}} + \frac{d \times 10^{(E-E_3')/59} + e + f \times 10^{(E_4'-E)/59}}{1 + 10^{(E-E_3')/59} + 10^{(E_4'-E)/59}} \quad (3)$$

In eqs 1 and 3, A is the total absorbance and a, b, and c are component absorbance values contributed by one flavin in the oxidized, semiquinone, and reduced states, respectively (FMN in the case of subunit D). In eq 3, d, e, and f are the corresponding absorbance components associated with the second flavin. E is the observed potential; E_1' and E_2' are the midpoint potentials for oxidized/semiquinone and semiquinone/reduced couples, respectively, for the first flavin, and E_3' and E_4' are the corresponding midpoint potentials for the second flavin. In eq 2, E is the observed potential and E_1' is the midpoint potential for the single-electron reduction of the 2Fe−2S cofactor. As above, A is the total absorbance, and the coefficients a and b in this case are the absorbance components associated with the oxidized and reduced forms of the iron−sulfur cluster, respectively.

In using eq 1 to fit the absorbance−potential data for the single-flavin (FMN) DHODB subunit D and for the A_{540} data within a limited range of potentials for the 2Fe−2S center in intact DHODB, the variables were unconstrained and regression analysis provided values in close agreement with those of the initial estimates. However, in using eq 3 to fit the data for the intact diflavin (FAD and FMN) DHODB, assumptions about the values of the absorbance components were made to prevent unrealistic fitting. The system is complex (four-electron titration with probable overlap of midpoint potentials) and was simplified by assuming that the oxidized and full reduced redox states of each flavin have an equal absorbance coefficient, specifically that $a = d$ and $c = f$. In this fitting process, values for the FMN potentials determined through analysis of the separate FMN-containing subunit D were initially fixed to allow estimates of the potentials for the FAD cofactor. After the initial round of fitting, these constraints were released and iterations produced estimates for both FAD and FMN potentials that were close to those obtained from the initial fit. In this fitting regime, the contribution from the 2Fe−2S cofactor (which has a very small absorption contribution at 453 nm and which is extensively reduced prior to considerable reduction of the flavins) was considered negligible in fitting the flavin potentials.

EPR and ENDOR Spectroscopy. During redox titrations with dithionite (see above), samples (200 μL) of DHODB (32.5 μM heterodimer) were withdrawn for EPR spectroscopic analyses. The samples were placed in standard 3 mm quartz EPR tubes, and sealed with Parafilm inside the glovebox. Immediately after the tubes had been removed from the glovebox, they were placed into a dry ice/ethanol bath to freeze the samples, and then transferred into liquid nitrogen. Samples were stored in liquid nitrogen until they were analyzed. The EPR spectra were recorded on a Bruker ELEXSYS E500 spectrometer fitted with an Oxford Instruments ESR9 liquid helium cryostat. ENDOR spectra were obtained at X-band using a Brucker ELEXSYS E500 spectrometer. To obtain samples with stronger EPR signals, more concentrated DHODB heterodimer samples were prepared (samples with concentrations between 267 and 279 μM were used). These samples were reduced using various amounts of concentrated dithionite, dihydroorotate, or NADH stock solutions. Samples were frozen in EPR tubes (as described above). All samples were contained in 100 mM potassium phosphate buffer (pH 7.0).

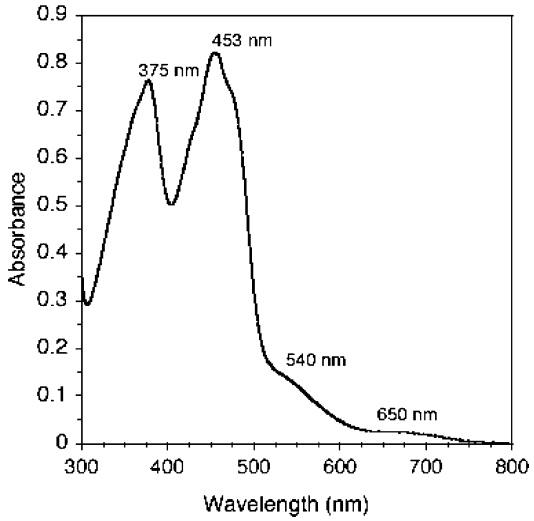

FIGURE 1: UV−visible spectrum of DHODB at a heterodimer (i.e., one catalytic and one electron transfer subunit) concentration of 22.9 μM. Positions of peaks and absorption features used in potentiometric titrations are indicated. Conditions: 50 mM potassium phosphate buffer (pH 7.0).

RESULTS

Spectral Properties of DHODB and Its Isolated Catalytic Dimer. Purified DHODB has absorption maxima at 273, 376, and 453 nm, and a shoulder at 540 nm. The middle two absorption features are typical of the spectra of flavin-containing enzymes with the 273 nm/453 nm ratio for the pure enzyme being ~3.15 (Figure 1). The extinction coefficients for the DHODB enzyme, calculated from measurement of the protein concentration by amino acid composition analysis and absorption at 453 and 540 nm, are as follows: $\epsilon_{453} = 36\,300$ M^{-1} cm^{-1} and $\epsilon_{540} = 5990$ M^{-1} cm^{-1}. In addition to these absorption maxima, there is a shoulder on the longer wavelength band at 475 nm. There is also a weak, broad absorption band with its center at the 650 nm region and extending toward 775 nm (Figure 1). The absorption pattern from 510 to 775 nm is specifically attributed to the 2Fe−2S center, since oxidized flavin does not absorb in this region. This absorption at longer wavelengths is absent in purified subunit D, which contains FMN only (see Figure 2A). The 272 nm/453 nm absorption ratio is ~3.5 for pure subunit D.

Redox Titration of the DHODB Subunit D Flavin. Previous studies have demonstrated the value of potentiometric analysis of component domains of complex multi-redox center enzymes (*13*, *14*, *19*). Such an approach allows accurate estimates of the reduction potentials of cofactors in isolation, and provides information regarding the spectral features accompanying their changes in redox state and any isosbestic points during the titration. These data are often

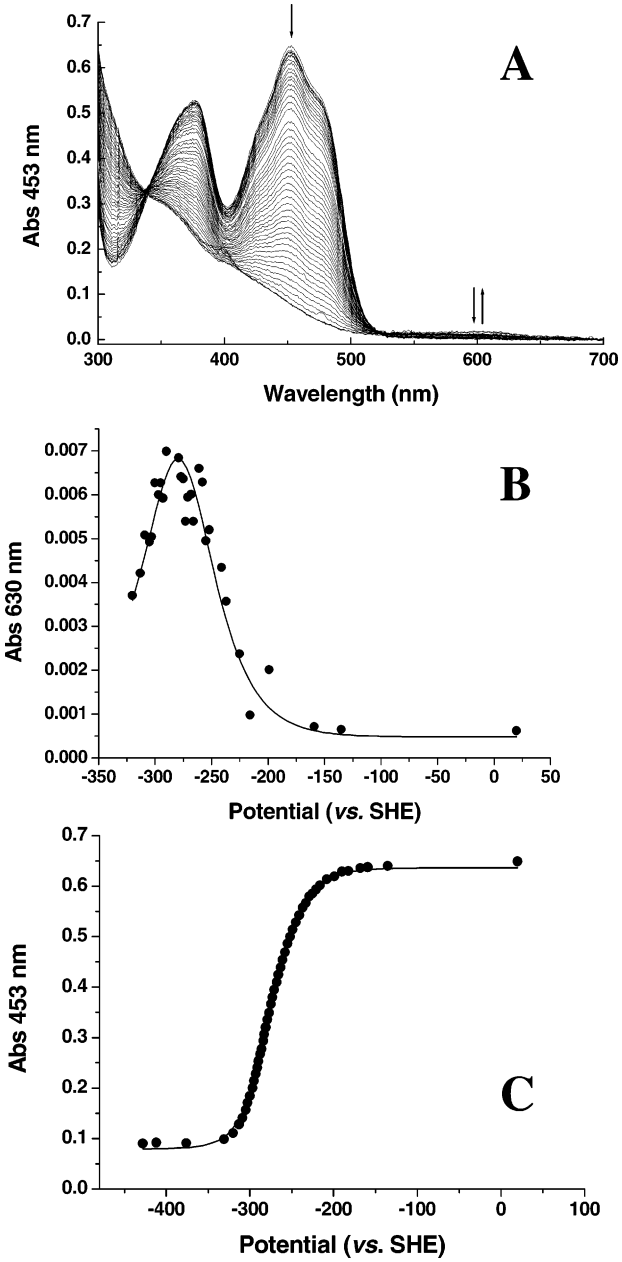

FIGURE 2: Redox titration of DHODB subunit D (FMN domain). (A) Spectra accumulated during redox titration of the FMN domain of DHODB. The most intense spectrum is that for the fully oxidized form of the FMN domain (ca. 70 μM), and other spectra of decreasing intensity report on the progressive reduction of the flavin from the quinone to the hydroquinone form with a dithionite reductant. Arrows indicate directions of absorption change at 453 nm (continuous decrease as the enzyme is progressively reduced) and 630 nm (accumulation, and then decay, of the neutral blue semiquinone form of the flavin). (B) Plot of the absorption at 630 nm vs the reduction potential for the redox titration of the DHODB FMN domain. Data are fitted to a two-electron Nernst function (eq 1), indicating the following midpoint reduction potentials: $E_1 = -298 \pm 4$ mV (for the addition of the first electron to the FMN) and $E_2 = -259 \pm 5$ mV for the addition of the second electron. (C) Plot of the absorption at 453 nm vs the reduction potential for the redox titration of the DHODB FMN domain. Data are fitted to a two-electron Nernst function (eq 1), indicating a midpoint reduction potential of -281 ± 5 mV for the two-electron reduction process.

critical for deconvoluting the redox properties of the intact complex enzymes. To allow a more accurate analysis of the properties of both flavin cofactors and the 2Fe−2S center in the intact DHODB enzyme, we first performed redox titrations with its D subunit, which contains only the FMN cofactor. Preliminary titrations indicated a tendency of the D subunit to aggregate over periods of several hours at 25 °C under the conditions that were used. However, negligible aggregation and associated turbidity were observed during titrations completed within approximately 5 h, and the results from these titrations are presented here. In addition, the titration was completely reversible, and spectra collected at the same potentials in oxidative and reductive directions were virtually identical. As shown in Figure 2A, the oxidized domain has typical flavin absorption maxima in the oxidized form at 453 and 377 nm, and reduction leads to bleaching of the absorption across the visible region. Close examination indicates the formation of a signal at a longer wavelength (centered at approximately 630 nm) typical of a neutral, blue semiquinone species. The maximal intensity of this spectral signal is very low, the maximal A_{630} being <2% of that of A_{453} for the oxidized flavin. The data suggest that the FMN does stabilize a semiquinone species. From this observation, the E_2 value (for the FMN semiquinone/reduced couple) could either be (i) slightly more negative than that of the E_1 value (for the oxidized/semiquinone couple) explaining the low intensity of the semiquinone signal (model 1) or (ii) slightly more positive than the E_1 value, again resulting in a very small amount of semiquinone stabilized during the redox titration (model 2). Figure 2B shows a plot of A_{630} versus potential data for DHODB subunit D fitted to eq 1. This produces the following estimates of the reduction potentials for the flavin according to model 1: $E_1 = -261 \pm 3$ mV and $E_2 = -309 \pm 10$ mV (i.e., the midpoint potential for the two-electron couple is approximately −285 mV). Alternatively, the estimates produced by assuming that the E_2 value is actually slightly more positive than E_1 (model 2) are -298 ± 4 mV (E_1) and -259 ± 5 mV (E_2) (i.e., the midpoint potential for the two-electron couple is approximately −278 mV). In favor of model 2 is the fact that the projected extinction coefficient for the FMN flavin semiquinone based upon this fitting regime is ∼1800 M^{-1} cm^{-1}, whereas that predicted by model 1 is <500 M^{-1} cm^{-1}. Clearly, model 2 is more consistent with typical extinction coefficients for a neutral blue semiquinone species. Thus, we consider that model 2 more accurately reflects the redox behavior of the FMN, and that the small amount of observed semiquinone is a consequence of the oxidized/semiquinone couple being ∼39 mV more negative than the semiquinone/hydroquinone couple. The absorption versus potential data at 453 nm (at which wavelength there is a much greater change in absorption) were also fitted to eq 1 (Figure 2C). At this wavelength, the fitting regime indicated that the potentials for both the oxidized/semiquinone and semiquinone/reduced couples were closely spaced and virtually within error of one another. The midpoint potential for the two-electron couple was -281 ± 5 mV, within error of that determined by analysis at 630 nm.

Redox Titration of DHODB. In contrast to results for subunit D, redox titrations with the DHODB heterodimer showed no problems with solution turbidity, despite the fact that certain titrations took up to 9 h for completion. The stability of the intact enzyme was particularly evident from the lack of change in the absorption at 800 nm between start and end spectra, reflecting an almost complete absence of

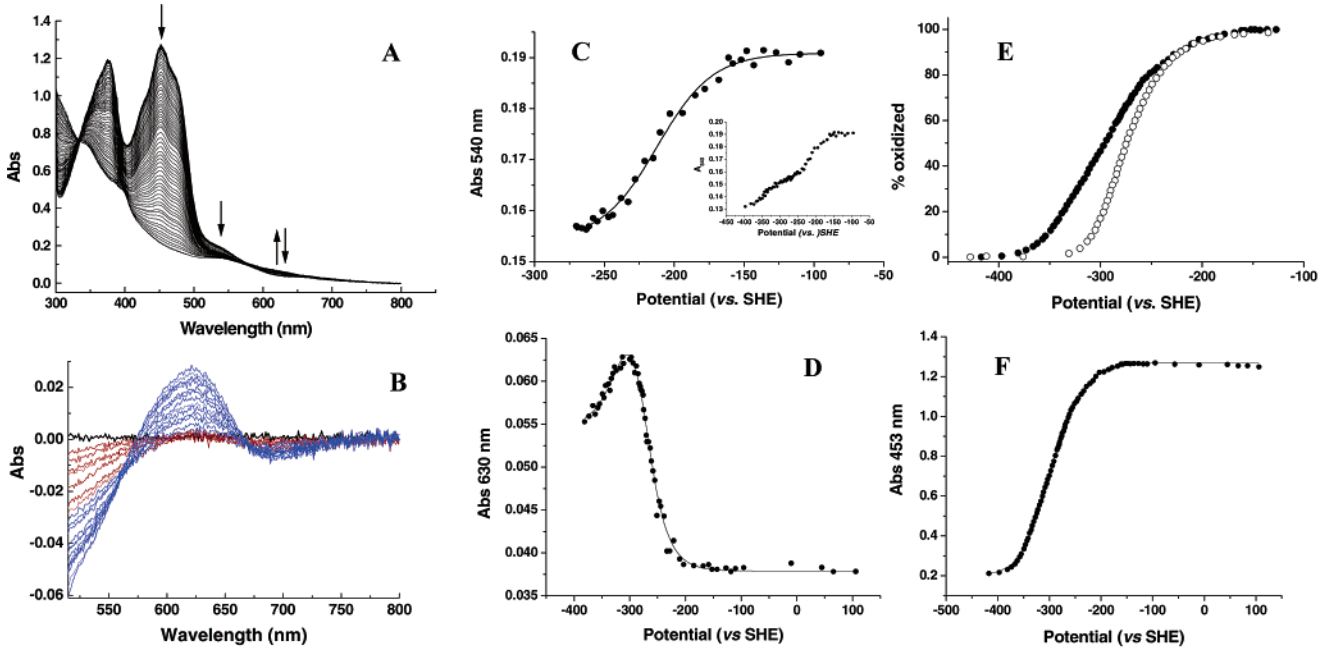

FIGURE 3: Spectral changes accompanying reduction of intact DHODB and potentiometric analysis. (A) Spectra accumulated during redox titration of intact DHODB are shown. The most intense spectrum is that for the fully oxidized form of the enzyme (ca. 35 μM), and other spectra of decreasing intensity report about the progressive reduction of both flavins and the 2Fe−2S center. Arrows indicate the directions of the absorption change at 453 nm (continuous decrease, predominantly from flavin absorption as the enzyme is reduced), 540 nm (bleaching of absorption from the 2Fe−2S center early in the reductive titration), and 630 nm (accumulation, and then decay, of the blue semiquinone form of the flavin cofactors). (B) Selected difference spectra generated by subtraction of successive absolute spectra recorded in the potential range between −118 and −300 mV from the absolute spectrum for the oxidized intact DHODB enzyme, using the data presented in panel A. The red spectra shown are recorded between −118 and −221 mV, and show decreased absorption at 540 nm (indicative of reduction of the iron−sulfur center), with negligible formation of a neutral semiquinone at 630 nm. The blue spectra are recorded between −228 and −300 mV, and show the buildup of the semiquinone signal at 630 nm to its maximum, together with the final stages of reduction of the iron−sulfur center at 540 nm. (C) Plot of the absorption at 540 nm vs the reduction potential for the redox titration of intact DHODB in the range from −100 to −275 mV. Data are fitted to a single electron Nernst function (eq 2) to describe the reduction of the 2Fe−2S center in the enzyme, indicating a midpoint reduction potential of −212 ± 3 mV for reduction of the cluster. The inset shows data points for the A_{540} vs potential over the entire range of the redox titration of intact DHODB. The upper phase is that fitted in the main figure and due to the reduction of the 2Fe−2S cluster. The lower phase is due to an absorption change from flavin cofactors as they become reduced at more negative reduction potentials. (D) Plot of absorption at 630 nm vs the reduction potential for the redox titration of intact DHODB. Data are fitted to a four-electron Nernst function (eq 3), indicating the following midpoint reduction potentials: $E_1 = -301 \pm 6$ mV for the addition of the first electron to the FMN (producing FMN semiquinone) and $E_2 = -252 \pm 8$ mV for the addition of the second electron (producing FMN hydroquinone) and $E_1 = -312 \pm 6$ mV and $E_2 = -297 \pm 5$ mV for the FAD. Values for the FMN are identical (within error) with those determined from analysis of the A_{630} data for the isolated FMN domain. (E) Overlay of the percentage oxidized enzyme vs potential data for the intact DHODB (●) and the isolated FMN domain (○). Data are scaled according to the proportion of the oxidized forms of the proteins based on the proportionate change in A_{453} between fully reduced and fully oxidized forms of the enzyme. (F) Fit of A_{453} data vs the reduction potential for the intact DHODB enzyme to a four-electron Nernst function (eq 3). With fixed values determined for the FMN cofactor from A_{630} data in the preliminary fitting regime (constraint is released after preliminary fitting rounds), the E_1 and E_2 couples for the FAD were both determined to be in the range of −328 ± 10 mV.

enzyme aggregation or spectral drift during the course of the titration.

The absorption spectrum for the oxidized DHODB enzyme exhibits typical flavoprotein features with absorption maxima at 376 and 453 nm. In addition, a distinct shoulder is observed at 540 nm, due to the minor absorption contribution from the 2Fe−2S cofactor. Reductive titration of DHODB leads to the bleaching of the absorption in the 540 nm region prior to any significant decrease in flavin absorption, suggesting that the 2Fe−2S center has the most positive reduction potential of all the redox centers in DHODB (Figure 3A). This assumption is borne out by examination of the difference spectra computed by subtraction of the starting (oxidized) spectrum of DHODB from those collected at subsequent points in the redox titration (Figure 3B). These show clearly that there is bleaching of the iron−sulfur center at 540 nm (red spectra) at more positive potentials, with the development of the semiquinone signal at 630 nm (blue spectra) occurring only after the iron−sulfur center is already significantly reduced. A plot of the A_{540} versus the reduction potential shows two distinct sigmoidal features (inset of Figure 3C). The first of these is essentially complete within the potential range between −130 and −230 mV (vs SHE). We assign this phase to the reduction of the 2Fe−2S cluster, and the fitting of a single electron Nernst function (eq 2) to the data in this regime indicates a reduction potential of −212 ± 3 mV (Figure 3C). As with the FMN domain, the titration was completely reversible and spectra collected at the same potentials in oxidative and reductive directions were virtually identical.

At a wavelength indicative of the formation of neutral, blue semiquinone species (630 nm), it is obvious that a signal accumulates in the redox titration of the intact DHODB. While the magnitude of the semiquinone signal remains low, the relative intensity of this signal (compared to the flavin content) is approximately twice that observed for the FMN domain. This suggests that either the FMN domain potentials are perturbed in the intact DHODB or the FAD cofactor also

contributes somewhat to the semiquinone signal that is obtained. A fit of the A_{630} versus potential data to a four-electron Nernst function (eq 3) produces estimates for the potentials of oxidized/semiquinone and semiquinone/hydroquinone couples of the FMN that are highly similar to those determined for the FMN cofactor in subunit D from similar data analysis ($E_1 = -301 \pm 6$ mV compared with -298 ± 4 mV for the isolated FMN domain; $E_2 = -252 \pm 8$ mV compared with -259 ± 5 mV for the isolated FMN domain) (Figure 3D). This fitting procedure also produces the following estimates for the FAD cofactor: $E_1 = -312 \pm 8$ mV and $E_2 = -297 \pm 6$ mV (i.e., a midpoint for the two-electron transition of the FAD of approximately -305 mV). As discussed above, the most likely explanation for the small semiquinone signal obtained during titrations of the FMN domain is that E_2 for the FMN is slightly more positive than E_1 (i.e., this model is more consistent with a typical coefficient for the neutral blue semiquinone). Similarly, the slightly increased semiquinone signal observed in titrations of intact DHODB is most likely related to a small contribution from the FAD (the FAD E_2 couple is slightly more positive than the E_1 couple, as with the FMN). It therefore appears that the potentials of the FMN are not considerably perturbed in the intact enzyme compared with the isolated FMN domain, and that the FAD produces some additional semiquinone (albeit at a more negative potential than the FMN), resulting in a slightly enhanced intensity of the semiquinone signal in intact DHODB.

Analysis of the absorption change at 453 nm (i.e., at the oxidized flavin maximum) as a function of the reduction potential for the intact DHODB enzyme indicates a smooth sigmoidal transition as both flavins are converted from quinone to hydroquinone forms (Figure 3E). There is no obvious breakpoint in the transition, suggesting that the potentials for the four redox couples of the two bound flavins are all relatively closely spaced, in agreement with the data from the A_{630} fit. The absence of any clear isosbestic points in the visible region during the reductive titration also indicates that the predominant flavin species that are observed are the quinone and hydroquinone forms, consistent with the fact that we observe only a very small proportion of semiquinone on the FMN during potentiometric titration of its domain, and predict a similar small semiquinone component for the FAD. In view of the fact that spin−spin coupling is observed by EPR spectroscopy at relatively positive potentials (see below), it appears likely that this phenomenon occurs due to interaction between the FMN semiquinone form and the reduced 2Fe−2S cluster. Thus, the FMN should be the flavin with the more positive potential, as predicted by fitting of data at 453 and 630 nm for the FMN domain, and at 630 nm for intact DHODB. Comparison of the forms of the A_{453} versus potential plots for intact DHODB and the FMN-containing domain (subunit D) bears out this hypothesis, since it is clear that the reductive titration of subunit D is complete by approximately -330 mV whereas the reduction of the intact DHODB is not completed until approximately -380 mV. To obtain further estimates of the reduction potentials for the flavin redox couples in intact DHODB, the A_{453} versus potential data were also fitted to the four-electron Nernst function (eq 3). The assumption was made that any minor absorption contribution from the 2Fe−2S center at this wavelength would occur only at the very oxidized end of the data, and would not have an impact on the estimates for the FAD redox couples. In the preliminary fitting regime, the E_1 and E_2 values for the first flavin (the FMN) were fixed according to the values determined from the A_{630} analysis (Figure 3F). The fitting procedure produced estimates for the E_1 and E_2 couples for the FAD that were nearly identical (both couples at -328 ± 10 mV, with E_2 slightly more positive than but within error of E_1). The A_{453} data thus predict a slightly more negative midpoint potential for the two-electron couple for the FAD than that obtained from the A_{630} data (-328 mV compared with -305 mV), but are again consistent with the FAD being the more negative flavin, and with its ability to produce only very small amounts of semiquinone during redox titration. While we cannot rule out the possibility that the potentials of the FMN are perturbed in the intact DHODB by comparison with the isolated FMN domain, it appears clear that any perturbations are relatively minor, and that the FMN has the more positive potential. Thus, on the basis of (i) the measured midpoint reduction potentials and (ii) the appearance of spin-coupled signals observed in our EPR studies (see below) at a relatively early stage in our redox titrations, we suggest that the spin-coupled state is attributed to interaction of the FMN semiquinone with the iron−sulfur center.

Reduction of DHODB and Subunit D by Dihydroorotate and NADH. Titration of DHODB by dihydroorotate affects the spectrum across the region below 775 nm (Figure 4A), but the spectral changes are more complicated than in the case of reduction by dithionite. A dihydroorotate−DHODB heterodimer molar ratio of approximately 5.6:1 is required to reduce DHODB to a level consistent with a two-electron-reduced enzyme produced using dithionite. An ∼200-fold molar excess of dihydroorotate to the DHODB heterodimer was required to decrease the absorbance at 453 nm by ∼66% of the maximum possible decrease achieved using dithionite, which can be extrapolated to indicate reduction to the four-electron level by dihydroorotate. Reduction of DHODB by NADH also affects the spectrum across the region below 775 nm (Figure 4B). A lower relative molar NADH concentration is required to reduce the enzyme to comparable redox states produced using dihydroorotate. An NADH:DHODB heterodimer molar ratio of ∼1.2:1 produces the spectrum typical of the two-electron-reduced form. At a 3.4-fold molar excess of NADH to DHODB heterodimer, the spectral change at 453 nm typical of the four-electron-reduced form is produced. Titration of subunit D with dihydroorotate confirms the identity of the catalytic subunit (Figure 4C). The decrease in absorbance at 453 nm was only attained with high substrate concentrations. After a more than 18-fold molar excess of dihydroorotate had been added to DHODB subunit D, the absorbance at 453 nm was decreased by ∼83% of the maximum achievable using excess dithionite. During the titration, absorption at long wavelengths (500−700 nm) develops with dihydroorotate as the reductant, suggesting the presence of either some semiquinone, some charge transfer character, or a combination of both spectral signals.

EPR Spectroscopy. In EPR studies, titration of DHODB with sodium dithionite produced the spectra shown in Figure 5A. As the dithionite concentration is increased, two signals become visible. First, the rhombic signal with g values of

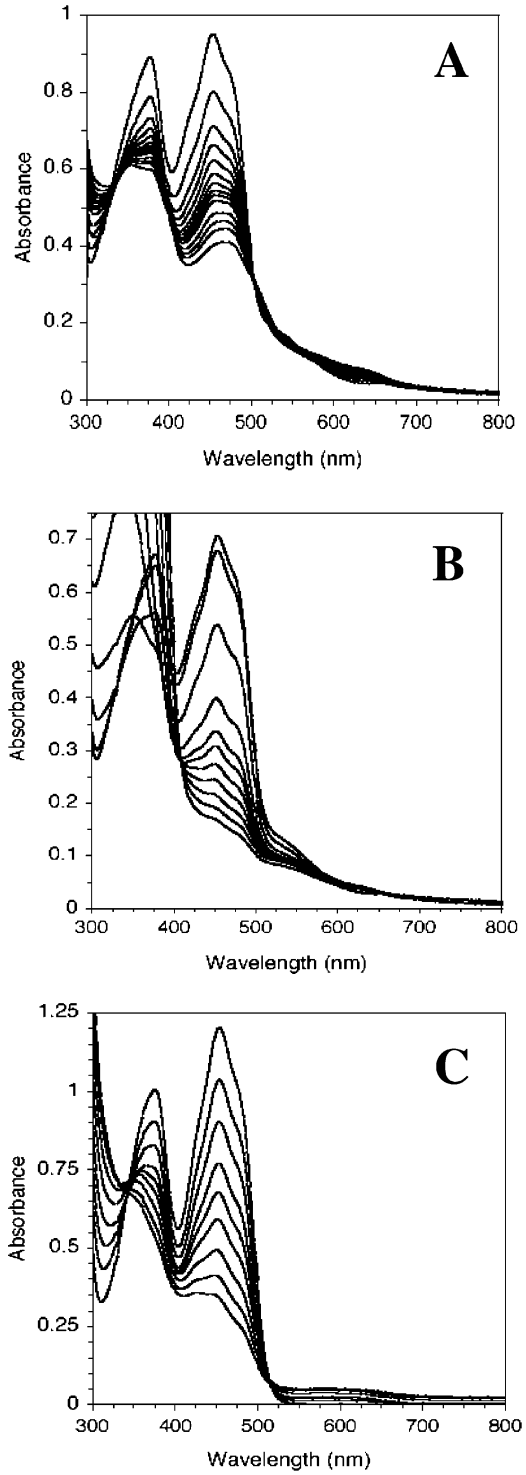

FIGURE 4: Spectral changes accompanying reduction of intact DHODB and the FMN domain using dihydroorotate and NADH. (A) Reduction of DHODB monitored by absorption spectroscopy following addition of dihydroorotate. Dihydroorotate concentrations, from top to bottom, were 0, 0.05, 0.10, 0.15, 0.20, 0.03, 0.40, 0.50, 0.59, 0.79, 1.17, 1.92, 3.36, and 5.99 mM. The DHODB heterodimer concentration was 26.5 μM. (B) Changes in the DHODB spectrum induced by adding various amounts of NADH. NADH concentrations, from top to bottom, were 0, 0.01, 0.02, 0.03, 0.04, 0.12, 0.24, 0.43, 0.89, 1.58, and 2.49 mM. The DHODB heterodimer concentration was 19.3 μM. (C) Changes in the DHODB subunit D spectrum upon addition of dihydroorotate. Dihydroorotate concentrations, from top to bottom, were 0, 0.04, 0.08, 0.16, 0.329, 0.69, 1.45, 2.30, and 3.57 mM. The subunit D concentration was ~125 μM. All titrations were carried out in 50 mM potassium phosphate (pH 7.0) under anaerobic conditions at 25 °C.

2.04, 1.95, and 1.89 is observed at 0.5 electron equivalent. The *g* values indicate that this signal arises from the reduced 2Fe−2S center (*16*). Second, another signal with a very small rhombic anisotropy and *g* values of 2.02, 1.99, and 1.96 (see Figure 5B) is first observed after the addition of 1.0 electron equivalent of dithionite. This signal grows to a maximum after the addition of 3.0 electron equivalents and then decreases with the addition of further dithionite. The anisotropy of this second signal is too small for it to arise from a reduced 2Fe−2S center. However, the only other redox centers in DHODB are flavins, the flavosemiquinone forms of which produce an isotropic signal (*17*). It is possible that this second signal is formed from the interaction between a reduced 2Fe−2S center and a flavosemiquinone via spin coupling. The components of such coupled signals can be separated if they have different temperature dependences. Flavosemiquinone signals can be observed up to room temperature, whereas 2Fe−2S signals are typically not observed above 100 K (*16*). Figure 6 shows the EPR spectra of DHODB reduced with 3.0 equiv of dithionite obtained at a series of temperatures. The spin-coupled signal is observed at 15 K, and its magnitude decreases in parallel with that of the 2Fe−2S signal as the temperature is increased to leave a single isotropic signal at 120 K. This isotropic signal has a g_{av} of 2.0032 and a peak-to-peak line width of 28 G. The *g* value and the lack of anisotropy are typical of a flavosemiquinone, but the line width is greater than those previously reported for such radicals (*17*). However, microwave power saturation experiments (data not shown) suggest that this isotropic signal relaxes much more rapidly than expected for an isolated radical, so there may be some residual coupling to the 2Fe−2S center which results in the increased line width. Neutral ("blue") and anionic ("red") flavosemiquinones are distinguished in EPR by their line widths, which cannot be used here due to the residual spin coupling interaction.

The number of electrons contributing to the EPR signals observed during dithionite titration can be determined using double integration of the EPR signals. The proportion of the spin-coupled signal was determined by subtracting fractions of the "2Fe−2S only" signal produced at high dithionite concentrations to produce difference spectra, as shown in Figure 5B. These difference spectra can then be integrated using the maximal 2Fe−2S signal as a standard and assuming that the spin-coupled signal is an $S = 1$ state [comparative integration between signals with different spin states requires a correction factor of $S(S + 1)$ as described in ref *28*]. These double integration data are plotted in Figure 7. If we assume that the assignment of the spin-coupled signal is correct, Figure 7 shows that more flavosemiquinone is formed at the cryogenic temperatures employed in EPR than in the room-temperature spectrophotometric dithionite reduction experiments (Figure 3A). At two electron equivalents, the spin-coupled signal amounts to half of one electron which, given that this is a spin-coupled signal proposed to be formed by equal contributions from a flavosemiquinone and a 2Fe−2S center, equates to a 25% yield of flavosemiquinone.

Reduction of DHODB using an excess of NADH or dihydroorotate produces EPR spectra that are distinct from those produced by dithionite. Reduction with 10.0 electron equivalents of dithionite produces the spectrum in Figure 8A, which shows only the 2Fe−2S signal at maximum

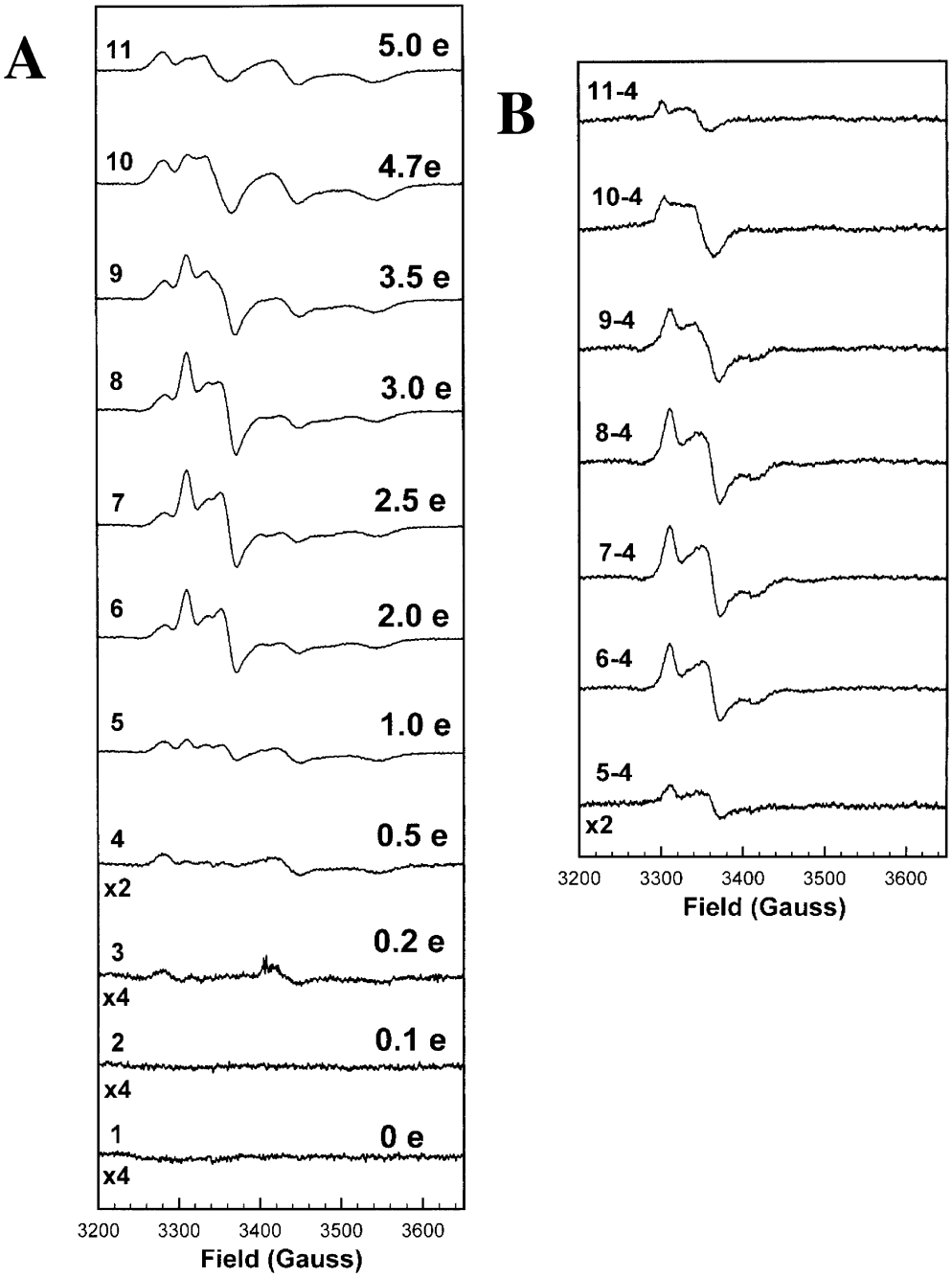

FIGURE 5: EPR spectra for DHODB in different states of reduction. (A) EPR spectra of DHODB titrated with sodium dithionite. The numbers to the right of the spectra are electron equivalents of sodium dithionite added, and the numbers to the left are spectrum identifiers. (B) Difference EPR spectra. The numbers show the spectra used to construct the differences. Different multiples of spectrum 4 were subtracted in each case until the contribution to the difference from the 2Fe−2S signal of spectrum 4 is minimized. Experimental conditions: microwave power of 200 μW, modulation amplitude of 4 G, modulation frequency of 100 kHz, and temperature of 20 K. The protein concentration was 32.5 μM.

intensity. Reduction with 10 equiv of NADH (effectively 20 electron equivalents) gives rise to the spectrum in Figure 8B, which shows mainly the 2Fe−2S signal, but also significant formation of the spin-coupled signal amounting to approximately 25% of one electron. Reduction with 10 equiv of dihydroorotate (again effectively 20 electron equivalents) produces the spectrum in Figure 8C. There are several differences between this spectrum and that produced by dithionite reduction shown in Figure 8A. First, the *g* values exhibited by the 2Fe−2S signal are altered by dihydroorotate reduction to 2.03, 1.94, and 1.90; i.e., the rhombic anisotropy is reduced relative to that observed with dithionite reduction. Such differences arise from changes in the geometry of the cysteine ligands to the 2Fe−2S center (*18*). A second difference is evident in the proportions of spin-coupled and 2Fe−2S signal present, with the spin-coupled signal accounting for 50% of the observed EPR signals. This suggests that binding of dihydroorotate (or possibly the product orotate) causes a change in the structure of the protein leading to related changes in the midpoint potentials of the redox centers. The structural change is consistent with published X-ray crystallographic studies (*5*).

ENDOR Spectroscopy. The ENDOR spectrum of the flavosemiquinone formed by reduction of DHODB with

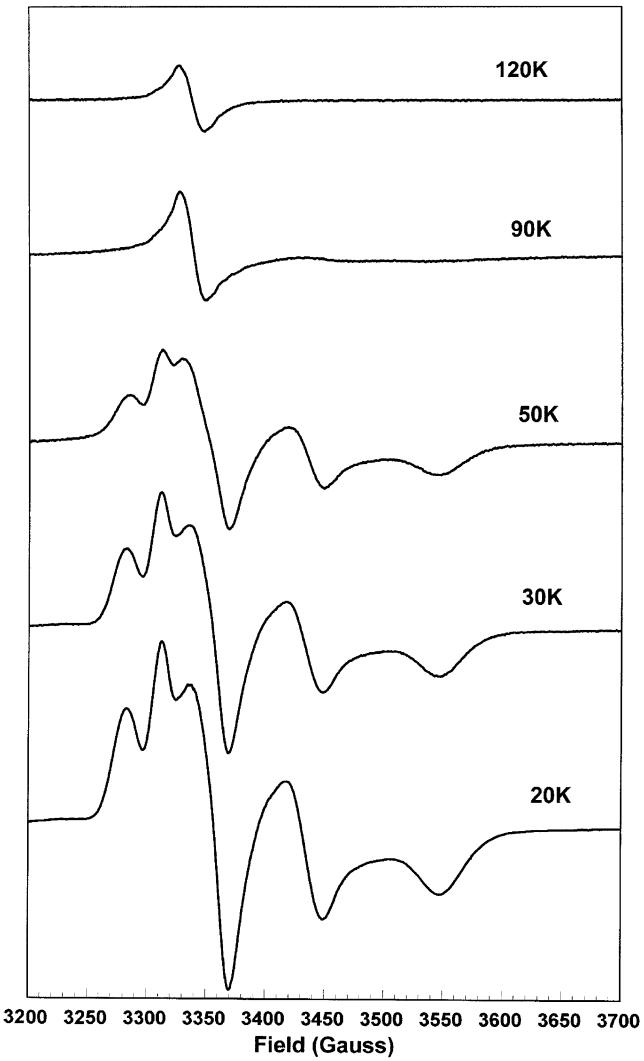

FIGURE 6: EPR spectra of DHODB reduced with three electron equivalents of sodium dithionite, recorded at the indicated temperatures. Experimental conditions: microwave power of 200 μW, modulation amplitude of 4 G, modulation frequency of 100 kHz, and temperature of 20 K. The protein concentration was ~270 μM.

dihydroorotate is shown in Figure 9. This region of the ENDOR spectrum shows features arising from hyperfine coupling to proton (hydrogen) nuclei. Frozen solution ENDOR spectra of radicals taken at the EPR crossing point typically show all orientations of the molecules in the external field simultaneously (i.e., a powder spectrum). Therefore, the line shapes observed reflect the symmetry of the hyperfine tensors and the random orientation of the tensors in the applied field. The hyperfine coupling constants (hfccs) determined from this spectrum are listed in Table 1, where they are compared with those previously reported for the neutral flavosemiquinone in a hydrogen bonding solvent. These values are in close agreement, confirming the assignment of the EPR spectrum to a flavosemiquinone. This comparison also shows that a neutral blue flavosemiquinone is formed, as anionic red flavosemiquinones exhibit different hfccs. That the hfccs exhibited by DHODB are so close to those measured for a neutral flavosemiquinone in water, which forms several hydrogen bonds to solvent, suggests that the flavosemiquinone formed in DHODB is hydrogen bonded to the protein. The flavosemiquinones formed using dithionite or NADH reduction have proven to be resistant to ENDOR

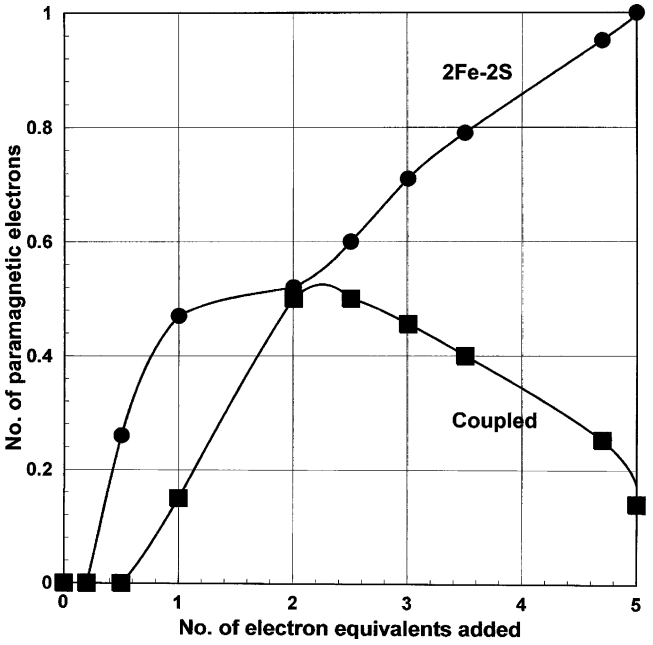

FIGURE 7: Plot of the number of paramagnetic electrons during titration of DHODB with sodium dithionite. The number of electrons was determined from the EPR signal double integral, and is plotted against the number of electron equivalents of sodium dithionite added. The numbers of paramagnetic electrons attributed to the 2Fe−2S signal and to the coupled signal are indicated with circles and squares, respectively. The protein concentration was 32.5 μM.

analysis due to residual interaction between the flavosemiquinone and 2Fe−2S center.

DISCUSSION

Potentiometric studies of diflavin enzymes using spectroelectrochemical methods are complicated by the similar absorption properties of the two flavin cofactors. We have previously used a domain dissection approach to measure the redox potentials of redox active domains in a number of mammalian and bacterial diflavin reductase enzymes, which has assisted in the assignment of measured redox potentials in the intact enzyme (*13*, *14*, *19*). We have now extended this approach to studies of DHODB, which has the added complication of a third redox cofactor in the form of a 2Fe−2S center. Potentiometry of the isolated catalytic subunit (subunit D) has assisted us in our assignment of the flavin redox potentials in DHODB, and EPR spectroscopy has enabled assignment of the potential for the 2Fe−2S center.

The EPR spectra observed on titration with sodium dithionite (Figure 5) allow for at least a qualitative analysis of the cofactor redox properties in DHODB at low temperatures, although the data (see Figure 7) are too sparse for accurate fitting. The 2Fe−2S center is reduced first, having the most positive potential, followed by the reduction of FMN, producing an amount of flavosemiquinone. In the portion of the titration in which the iron−sulfur center is reduced, it is predominantly the FMN cofactor that also undergoes reduction, and which should spin couple with the 2Fe−2S center. Later in the redox titration, the FAD is reduced, and also appears to produce a small amount of flavosemiquinone. However, at these potentials, the signal indicating spin coupling is decaying, suggesting strongly that the FMN is the sole flavin which couples with the 2Fe−2S

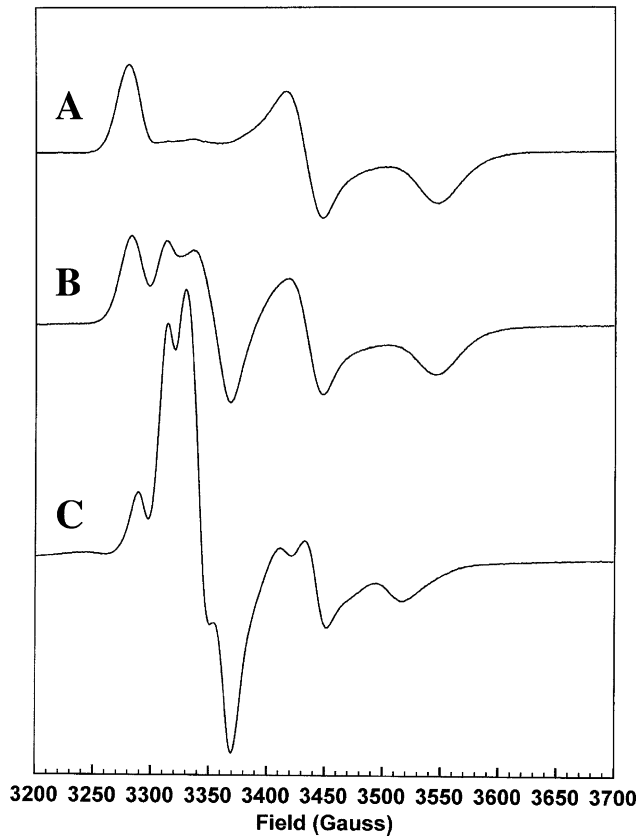

FIGURE 8: EPR spectra of DHODB reduced with different compounds. DHODB was reduced with 10 electron equivalents of sodium dithionite (A), 10 equiv (20 electron equivalents) of NADH (B), and 10 equiv (20 electron equivalents) of dihydroorotate (C). Experimental conditions: microwave power of 200 μW, modulation amplitude of 4 G, modulation frequency of 100 kHz, and temperature of 20 K. The protein concentration was ~270 μM.

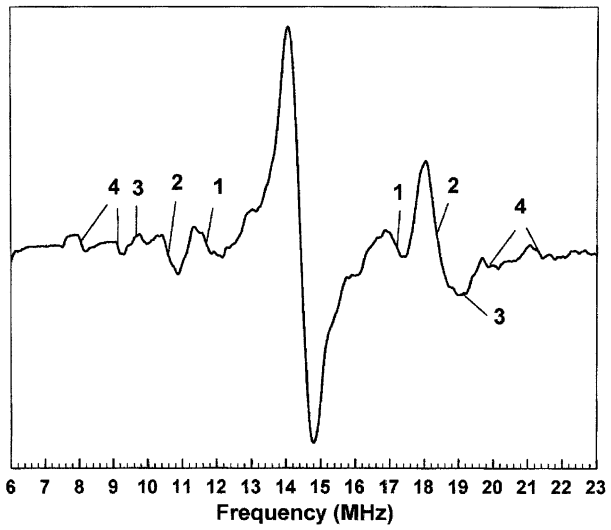

FIGURE 9: ENDOR spectra of DHODB reduced with 10 equiv of dihydroorotate. The numbering scheme refers to features identified in Table 1. Experimental conditions: microwave power of 1 mW, radiofrequency power of 100 W, radiofrequency modulation depth of 158 kHz, temperature of 140 K, and sum of 100 scans. The protein concentration was ~270 μM.

center. However, the EPR data show a level of flavosemiquinone formation (25%) much higher than that detected optically. This could arise from a temperature-dependent process within the protein, possibly a change in the conformation of the protein or a change in the protonation equilibrium between residues close to the flavin leading to a decrease in the potential of the semiquinone/hydroquinone couple. These data do not allow a determination of the process involved, but even a modest change in the E_1 and E_2 couples for the flavins would cause reasonably large alterations in the proportions of flavosemiquinone stabilized according to our potentiometric data. It is also possible that the presence of mediators in the optical titrations allows for the disproportionation of a thermodynamically unstable, but kinetically stable, flavosemiquinone.

Table 1: Assignment of ENDOR Spectral Features

feature	DHODB hyperfine coupling constant (MHz)	flavin neutral semiquinone hyperfine coupling constant (MHz)	assignment
1	−5.5	−5.5	6H
2	7.7	7.4	8MeA$_+$
3	9.6	9.7	8MeA$_{\|\|}$
4	10.9	not known	C(1′)H
	13.2	not known	C(1′)H

The most striking feature of the sodium dithionite titration (Figure 5) is the formation of the coupled signal (see Figures 5 and 8). There are no well-characterized flavosemiquinone−2Fe−2S coupled signals in the literature. However, some clues concerning the formation and behavior of this signal may be derived from flavosemiquinone−4Fe−4S coupled species such as that found in trimethylamine dehydrogenase (TMADH) (*20*, *21*). In TMADH, the triplet coupled signal arises from an antiferromagnetically coupled 1:1 mixture of reduced 4Fe−4S center and flavosemiquinone, and is broader than the uncoupled 4Fe−4S signal at ~400 G wide. The coupled signal in DHODB is narrower than the uncoupled 2Fe−2S signal at ~60 G, but does appear as a "triplet". This reflects the differences in the iron−sulfur cluster structure, differences in the relative orientations of the coupled redox centers, and the distances between the coupled species, 4.5 Å in TMADH (*22*) and 7.8 Å in DHODB (*6*) (both distances represent the closest approach between atoms from each cofactor), which leads to weaker coupling in DHODB but suggests that a similar coupling mechanism may operate in both systems. These differences may also be responsible for our failure to detect in DHODB the "half-field" signal at ~1500 G which is characteristic of the spin-coupled state of TMADH. Phthalate dioxygenase reductase (PDR) contains a 2Fe−2S center and a FMN cofactor that stabilizes a flavosemiquinone. The center-to-center distance between the cofactors in PDR is 12 Å, comparable with the distance of 12.7 Å in DHODB. However, PDR does not give a coupled signal due to the relative orientation of the 2Fe−2S center and the FMN (*23*). It has been suggested that the electron superexchange paths that allow for coupling between centers also contribute to the efficiency of electron transfer between them (*24*). Thus, observation of a coupled signal in DHODB suggests that the protein is structured to allow for efficient electron transfer between the FMN and the 2Fe−2S center. The impact of site-directed mutants on electron transfer rates might therefore also be reflected in the coupling between the redox centers.

The coupled signal observed in EPR spectra of DHODB reduced with dihydroorotate (Figure 8) is slightly narrower than that formed by sodium dithionite reduction. This form

presumably has orotate bound at the FMN site. The narrowing of the signal reflects a decrease in the degree of coupling between the FMN flavosemiquinone and the 2Fe−2S center. The argument presented above (*24*) would suggest that such a decrease would inhibit the back reaction between the reduced 2Fe−2S center and flavosemiquinone with product bound and provide some directionality (gating) to the electron transfer path. However, the structure of the 2Fe−2S center is also altered in dihydroorotate-reduced samples, as reflected in the *g* values for this center, so the decreased level of coupling could be a reflection of this structural change. In either case, it is clear that the changes observed in the X-ray crystal structure on dihydroorotate−orotate binding (*5*) affect the EPR spectra and that these changes will have an impact on electron transfer.

The ENDOR spectrum of the flavosemiquinone formed in dihydroorotate-reduced DHODB (Figure 9) exhibits hyperfine coupling typical of a neutral (blue) species (*25*). This is consistent with the optical data and obviates the need to depend on EPR line width as an indicator of the species that is formed. It also removes any possibility that some anionic flavosemiquinone is formed and is not detected in the optical spectra due to overlap with 2Fe−2S bands. The hfcs are consistent with those of "free" neutral flavosemiquinones in hydrogen bonding solvent (*26*). This consistency is remarkable given the X-ray crystal structure of the DHODB−orotate complex which shows the reorientation of Lys48 on orotate binding and the formation of hydrogen bonds between Lys48 and N(5) and O(4) of the FMN (*5*). The presence of the presumed positively charged residue does not lead to ionization of the FMN and formation of the anionic flavosemiquinone, nor does it lead to an unusual unpaired electron spin distribution as reflected in the hfccs. This suggests that the charge on Lys48 is completely compensated by the negative charge on the bound orotate and that the FMN site has evolved to allow for such compensation without an impact on flavin function. Ideally, we would like to compare the ENDOR spectrum of the flavosemiquinone formed in the dihydroorotate-reduced enzyme with that of the dithionite-reduced form. Unfortunately, residual dipolar coupling between the 2Fe−2S cluster and the flavosemiquinone in the latter, similar to that observed between the flavosemiquinone and iron−sulfur cluster N3 in respiratory Complex I (*27*), has prevented us from obtaining meaningful ENDOR data for any species other than the dihydroorotate-reduced form.

In summary, our potentiometric analysis indicates that all of the redox centers in DHODB titrate in the range of −200 to −320 mV. These values are consistent with the electron transfer from dihydroorotate [ca. −470 mV (*29*)] and NAD^+ (−320 mV). The detailed thermodynamic basis for electron transfer in DHODB reported herein provides a framework for transient kinetic studies of electron transfer. We are currently pursuing this aspect of the enzymology of DHODB.

REFERENCES

1. Kahler, A. E., Nielsen, F. S., and Switzer, R. L. (1999) Biochemical characterization of the heteromeric *Bacillus subtilis* dihydroorotate dehydrogenase and its isolated subunits, *Arch. Biochem. Biophys. 371*, 191−201.
2. Argyrou, A., Washabaugh, M. W., and Pickart, C. M. (2000) Dihydroorotate dehydrogenase from *Clostridium oroticum* is a class 1B enzyme and utilizes a concerted mechanism of catalysis, *Biochemistry 39*, 10373−10384.
3. Nielsen, F. S., Andersen, P. S., and Jensen, K. F. (1996) The B form of dihydroorotate dehydrogenase from *Lactococcus lactis* consists of two different subunits, encoded by the pyrDb and pyrK genes, and contains FMN, FAD, and [FeS] redox centers, *J. Biol. Chem. 271*, 29359−29365.
4. Marcinkeviciene, J., Tinney, L. M., Wang, K. H., Rogers, M. J., and Copeland, R. A. (1999) Dihydroorotate dehydrogenase B of *Enterococcus faecalis*. Characterization and insights into chemical mechanism, *Biochemistry 38*, 13129−13137.
5. Rowland, P., Norager, S., Jensen, K. F., and Larsen, S. (2000) Structure of dihydroorotate dehydrogenase B: electron transfer between two flavin groups bridged by an iron-sulphur cluster, *Struct. Folding Des. 8*, 1227−1238.
6. Rowland, P., Bjornberg, O., Nielsen, F. S., Jensen, K. F., and Larsen, S. (1998) The crystal structure of *Lactococcus lactis* dihydroorotate dehydrogenase A complexed with the enzyme reaction product throws light on its enzymatic function, *Protein Sci. 7*, 1269−1279.
7. Hines, V., and Johnston, M. (1989) Mechanistic studies on the bovine liver mitochondrial dihydroorotate dehydrogenase using kinetic deuterium isotope effects, *Biochemistry 28*, 1227−1234.
8. Pascal, R. A., Jr., and Walsh, C. T. (1984) Mechanistic studies with deuterated dihydroorotates on the dihydroorotate oxidase from *Crithidia fasciculata*, *Biochemistry 23*, 2745−2752.
9. Palfey, B. A., Bjornberg, O., and Jensen, K. F. (2001) Insight into the chemistry of flavin reduction and oxidation in *Escherichia coli* dihydroorotate dehydrogenase obtained by rapid reaction studies, *Biochemistry 40*, 4381−4390.
10. Palfey, B. A., Bjornberg, O., and Jensen, K. F. (2001) Specific inhibition of a family 1A dihydroorotate dehydrogenase by benzoate pyrimidine analogues, *J. Med. Chem. 44*, 2861−2864.
11. Bjornberg, O., Jordan, D. B., Palfey, B. A., and Jensen, K. F. (2001) Dihydrooxonate is a substrate of dihydroorotate dehydrogenase (DHOD) providing evidence for involvement of cysteine and serine residues in base catalysis, *Arch. Biochem. Biophys. 391*, 286−294.
12. Argyrou, A., and Washabaugh, M. W. (1999) Proton transfer from the C_5-proR/proS positions of L-dihydroorotate: general-base catalysis, isotope effects, and internal return, *J. Am. Chem. Soc. 121*, 12054−12062.
13. Daff, S. N., Chapman, S. K., Turner, K. L., Holt, R. A., Govindaraj, S., Poulos, T. L., and Munro, A. W. (1997) Redox control of the catalytic cycle of flavocytochrome P-450 BM3, *Biochemistry 36*, 13816−13823.
14. Munro, A. W., Noble, M. A., Robledo, L., Daff, S. N., and Chapman, S. K. (2001) Determination of the redox properties of human NADPH-cytochrome P450 reductase, *Biochemistry 40*, 1956−1963.
15. Dutton, P. L. (1978) Redox potentiometry: determination of midpoint potentials of oxidation−reduction components of biological electron-transfer systems, *Methods Enzymol. 54*, 411−435.
16. Dalton, L. R. (1985) *EPR and Advanced EPR Studies of Biological Systems*, CRC Press, Boca Raton, FL.
17. Massey, V., and Palmer, G. (1966) On the existence of spectrally distinct classes of flavoprotein semiquinones. A new method for the quantitative production of flavoprotein semiquinones, *Biochemistry 5*, 3181−3189.
18. Bertrand, P., and Gayda, J. P. (1979) A theoretical interpretation of the variations of some physical parameters within the [2Fe-2S] ferredoxin group, *Biochim. Biophys. Acta 579*, 107−121.
19. Wolthers, K. R., Basran, J., Munro, A. W., and Scrutton, N. S. (2003) Molecular dissection of human methionine synthase reductase: determination of the flavin redox potentials in full-length enzyme and isolated flavin-binding domains, *Biochemistry 42*, 3911−3920.
20. Rohlfs, R. J., Huang, L., and Hille, R. (1995) Prototropic control of intramolecular electron transfer in trimethylamine dehydrogenase, *J. Biol. Chem. 270*, 22196−22207.
21. Fournel, A., Gambarelli, S., Guigliarelli, B., More, C., Asso, M., Chouteau, G., Hille, R., and Bertrand, P. (1998) Magnetic interactions between a 4Fe-4S cluster and a flavin mononucleotide radical in the enzyme trimethylamine dehydrogenase: a high field electron paramagnetic resonance study, *J. Chem. Phys. 109*, 10905−10912.

22. Trickey, P., Basran, J., Lian, L. Y., Chen, Z., Barton, J. D., Sutcliffe, M. J., Scrutton, N. S., and Mathews, F. S. (2000) Structural and biochemical characterization of recombinant wild type and a C30A mutant of trimethylamine dehydrogenase from *Methylophilus methylotrophus* (sp. W3A1), *Biochemistry 39*, 7678−7688.
23. Bertrand, P., More, C., and Camensuli, P. (1995) Evidence for a magic magnetic configuration between FMN and the 2Fe-2S center of phthalate dioxygenase reductase of *Pseudomonas cepacia*, *J. Am. Chem. Soc. 117*, 1807−1809.
24. Bertrand, P. (1991) Application of electron-transfer theories to biological systems, *Struct. Bonding 75*, 3−47.
25. Weilbacher, E., Helle, N., Elsner, M., Kurreck, H., Müller, F., and Allendoefer, R. D. (1988) ^{1}H, ^{2}H, ^{19}F, ^{14}N ENDOR and TRIPLE resonance investigations of substituted flavin radicals in their different protonation states, *Magn. Reson. Chem. 26*, 64−72.
26. Kurreck, H., Bretz, N. H., Helle, N., Henzel, N., and Weilbacher, E. (1988) ENDOR studies of flavins and flavoproteins, *J. Chem. Soc., Faraday Trans. 84*, 3293−3306.
27. Sled, V. D., Rudnitzky, N. I., Hatefi, Y., and Ohnishi, T. (1994) Thermodynamic analysis of flavin in mitochondrial NADH: ubiquinone oxidoreductase (complex I), *Biochemistry 33*, 10069−10075.
28. Weil, J. A., Bolton, J. R., and Wertz, J. A. (1994) *Electron Paramagnetic Resonance: Elementary Theory and Practical Applications*, John Wiley and Sons: New York, p 498.
29. Calvo Blazquez, L., Rodriguez Flores, J., Vinagre Jara, F., and Sanchez Misiego, A. (1990) Determination of orotic acid (vitamin B_{13}) in milk by differential pulse polarography (DPP), *Fresenius' J. Anal. Chem. 338*, 80−81.

BI036179I